Using uncertainty to link edge detection and local surface modelling

Olivier Monga, Nicholas Ayache, Peter Sander

USING UNCERTAINTY TO LINK 3D EDGE DETECTION AND LOCAL SURFACE MODELLING

O Monga, N Ayache, P Sander

INRIA Domaine de Voluceau-Rocquencourt - B.P. 105
78153 Le Chesnay Cedex, France

Abstract

We establish a theoretical link between the 3D edge detection and the local surface approximation using uncertainty. As a practical application of the theory, we present a method for computing typical curvature features from 3D medical images. We use the uncertainties inherent in edge (and surface) detection in 2- and 3-dimensional images determined by quantitatively analyzing the uncertainty in edge position, orientation and magnitude produced by the multidimensional (2-D and 3-D) versions of the Monga-Deriche-Canny recursive separable edge-detector. These uncertainties allow to compute local geometric models (quadric surface patches) of the surface, which are suitable for reliably estimating local surface characteristics, for example, Gaussian and Mean curvature. We demonstrate the effectiveness of our methods compared to previous techniques. These curvatures are then used to obtain more structured features such as curvature extrema and lines of curvature extrema. The final goal is to extract robust geometric features on which registration and/or tracking procedures can rely.

key words

Typical surface features, local curvature extrema, mean and Gaussian curvature, local surface modelling, uncertainty, 3D edge detection.

1 Introduction

Modern medical imaging techniques, such as Magnetic Resonance Imaging (MRI) or X-ray computed tomography provide three dimensional (3D) images of internal structures of the body, usually by means of a stack of tomographic images. In many applications, the physician asks for a segmentation of these 3D images into regions of interest he wants to manipulate, display, and characterize by objective measurements [AB+90]. The first stage in the automatic analysis of such data is 3D edge detection [ZH81, MD89, MDR91] which provide points corresponding to the boundaries of the surfaces forming the 3D structure. The next stage is to characterize the local geometry of these surfaces in order to extract points or lines on which registration and/or tracking procedures can rely [Koe90].

Sander and Zucker have proposed to compute surface singularities by the calculation of curvatures using local approximation and by iterative refinement of the curvature field [SZ87, SZ90]. In this paper we present a pipeline of processes which define a hierarchical description of the second order differential characteristics of the surfaces. We focus on the theoretical coherence of these levels of representation. Our levels of representation of the local geometry of the surfaces are :

- 3D edge points,
- Mean and Gaussian curvature, principal curvature directions,
- Local images of the curvatures,
- Characteristic points : curvature extrema, parabolic points, umbilic points ...

- Characteristic lines : Lines of curvature extrema, parabolic lines, Umbilic points ...

Three-dimensional edge detection is performed using recursive separable filters approximating the gradient or Laplacian as described in [MD89, MDR91, MDMC]. From these edge points we build an adjacency graph with position and gradient vector attached to each edge point.

To compute curvatures from this graph we fit a local model at the neighbourhood of each point. The local model is a quadratic surface and the fitting method is a Kalman filter. Our approximation scheme uses the locations of the edge points and also the gradient direction which approximates the normal to the surface. Using uncertainty we establish a theoretical link between the edge detection and the local surface approximation.

Our statistical results are then used as a solid theoretical foundation on which to base subsequent computations, such as, for example, the determination of local surface curvature using local geometric models or for surface segmentation [BJ88].

We tie the results of the analysis of the uncertainties involved in edge detection to the estimation of local geometric surfaces by a Kalman filtering technique. While the instantiation of these local models is similar to the method of Sander and Zucker [SZ90], the utilization of uncertainties yields improved results. In addition, Kalman filtering permits incremental and selective incorporation of new data, thus ensuring that the local models are fit to, and only to, relevant data points. We expect that this will permit us to effectively deal with the problem of discontinuities where the local surface smoothness assumptions break down.

From the local fitting, we calculate for each edge point a mean curvature, a gaussian curvature, and principal curvature directions, and covariance matrices defining the uncertainty. We define local curvature images by projecting at each point the curvatures of the neighbours onto the tangent plane. This yields the local aspect of the curvatures at a point.

From the curvature field we extract typical points such as curvature extrema, parabolic points, umbilic points ... This is done by using the local image of the curvatures defined at each (edge) point. For instance to select the extrema of the maximun curvature in the maximum curvature direction, we employ an algorithm very similar to the extraction of the extrema of the gradient magnitude in the gradient direction used in many 2D edge detection algorithms [Der87, Can86].

From these typical points, we extract characteristic lines such as line of mean curvature extrema, parabolic lines .... To obtain lines of mean curvature extrema, we perform a 3D hysteresis thresholding on the extrema curvature points using the mean curvature. Here again the algorithm is very similar to the one used to threshold the local gradient extrema described in [MDR91].

This work is described with more details in [MAS91].

2 Parametric local surface model

2.1 Problem formulation

In this section, we set up the local parametric surface models, describe briefly how to compute surface curvatures from the models, and present the problem of determining the parameters of the models from the data derived from the 3-D gradient operator. We thus assume that we are given the locations of estimated surface points P and their estimated surface normals $\mathbf{N}$ corresponding to the vector gradient, (see [MD89, MDR91] on how to compute them). Using $\mathbf{N}$ we can establish a *tangent plane coordinate system* at P, which we denote ($\mathbf{P}$, $\mathbf{Q}$, $\mathbf{N}$). Note that the basis ($\mathbf{P}$, $\mathbf{Q}$) of the tangent plane at P is arbitrary — the only constraint is that the coordinate system be right-handed and orthonormal.

In the following, P is the point at which the surface patch is being fit, and Q_i are neighbouring estimated surface points with associated normals $\mathbf{n}_i$, with both given in P's tangent plane coordinates (the development is simpler in these coordinates; we map everything into the actual image coordinates in §3.4.1).

2.2 Local geometric model

We assume that the data returned by the gradient operator represent noisy estimates of points and normals from a (smooth) surface $\mathcal{S}$. We treat a surface as a differentiable manifold and build local charts (parametrizations) at all the estimated surface points. Thus, at $P \in \mathcal{S}$ we assume that the local chart (ψ, U)

$$\psi : U \subset \mathcal{S} \rightarrow \mathbb{R}^2$$

(ψ a diffeomorphism, $P \in$ open set U) is such that $\psi(P) = (0,0)$ and its imbedding

$$\phi = i \circ \psi^{-1} : \psi(U) \subset \mathbb{R}^2 \rightarrow \mathbb{R}^3$$

in $\mathbb{R}^3$ (based on P's tangent plane coordinates) is the graph of some function $h : \psi(U) \rightarrow \mathbb{R}$ with

$$\begin{aligned} h(0,0) &= 0, \\ h_p(0,0) = \left.\frac{\partial h}{\partial p}\right|_{(0,0)} &= 0 \\ h_q(0,0) = \left.\frac{\partial h}{\partial q}\right|_{(0,0)} &= 0 \end{aligned}$$

(this is always true in some local chart). The Taylor expansion of h about the origin is

$$h(p,q) = \frac{1}{2}\left(h_{pp}p^2 + 2h_{pq}pq + h_{qq}q^2\right) + R.$$

Since our ultimate goal is computation of curvatures and related information, we take the simplest local chart which is appropriate, i.e., where

$$h = \frac{1}{2}ep^2 + fpq + \frac{1}{2}gq^2, \tag{1}$$

where we write

$$e = h_{pp}(0,0), \quad f = h_{pq}(0,0), \quad g = h_{qq}(0,0)$$

(known as a *parabolic quadric*).

2.3 Surface curvature

The curvature of the surface $\mathcal{S}$ at P can be computed from its local parametrization $\phi : \psi(U) \rightarrow \mathbb{R}^3$ in P's tangent plane coordinates. The surface normal at P is expressed as

$$\mathbf{N}(0,0) = \left.\frac{\phi_p \times \phi_q}{\|\phi_p \times \phi_q\|}\right|_{(0,0)}.$$

(In the following, we take it as understood that derivatives are evaluated at $(0,0)$, i.e., the $|_{(0,0)}$ is implicit.) The matrices

$$\begin{aligned} F_1 &= \begin{pmatrix} \langle \phi_p, \phi_p \rangle & \langle \phi_p, \phi_q \rangle \\ \langle \phi_q, \phi_p \rangle & \langle \phi_q, \phi_q \rangle \end{pmatrix}, \\ F_2 &= \begin{pmatrix} -\langle \phi_p, \mathbf{N}_p \rangle & -\langle \phi_p, \mathbf{N}_q \rangle \\ -\langle \phi_q, \mathbf{N}_p \rangle & -\langle \phi_q, \mathbf{N}_q \rangle \end{pmatrix}, \end{aligned}$$

are determined from the first and second fundamental forms respectively of the surface ($\langle \bullet, \bullet \rangle$ denotes inner product). The principal curvatures κ_1, κ_2 of ϕ at P in $(\mathbf{P}, \mathbf{Q}, \mathbf{N})$ coordinates are the two eigenvalues of the matrix $F_2 F_1^{-1}$, and the Gaussian and mean curvatures are

$$\begin{aligned} \kappa_g &= \kappa_1 \kappa_2, \\ \kappa_m &= \frac{\kappa_1 + \kappa_2}{2} \end{aligned}$$

respectively. We show how to compute uncertainties in the curvatures in §3.4.2.

3 Recursive estimation of surface parameters

3.1 Instantiating the model

Now, we wish to determine the local quadric surface passing through point P which "best" (in a sense made precise below) fits neighbouring points $Q_i = (p_i, q_i, n_i)^t$ and their normals $\mathbf{n}_i = (\alpha_i', \beta_i', \gamma_i')^t$. In P's tangent plane coordinate system, the equation of the quadric gives us a first measurement equation

$$E_1(e, f, g) = p_i^2 e + 2p_i q_i f + q_i^2 g - 2n_i = 0 \tag{2}$$

between the position of Q_i and the parameters e, f, g which are to be determined from the data.

In addition to estimated surface point locations, the 3-D gradient operator provides an estimate of gradient direction and we can use the measured normal $\mathbf{n}_i$ at point Q_i to further constrain the quadric surface parameters. We know that, in the tangent plane coordinates, the quadric's normal at point Q_i is

$$\mathbf{n}_i = \begin{pmatrix} -p_i e - q_i f \\ -p_i f - q_i g \\ 1 \end{pmatrix}.$$

Denoting the scaled normal *measured* at point Q_i by $(\alpha_i, \beta_i, 1)^t = (\alpha_i'/\gamma_i', \beta_i'\gamma_i', \gamma_i'/\gamma_i')^t$, we obtain two more measurement equations

$$E_2(e, f, g) = p_i e + q_i f + \alpha_i = 0, \tag{3}$$
$$E_3(e, f, g) = p_i f + q_i g + \beta_i = 0. \tag{4}$$

Equations (E_1–E_3) are the three measurement equations which constrain the determination of the parameters e, f, g of the quadric at point P. These equations should be compared to the four equations E_1'–E_4' of [SZ90]: Eq. E_1 is the same, but Eqs. (E_2' – E_4') there were based on unit normals and involved a non-linear combination of e, f, g. The only restriction on our equations here is the assumption that the normal $\mathbf{n}_i$ of Q_i measured in the tangent plane coordinates of P has a nonzero third component, which is reasonable if we assume that Q_i lies in the neighborhood of point P. (In fact, if the surface is regular, such a neighborhood exists [dC76, p.164], at least before discretization[1]). When this component vanishes, the local parametrization of the quadric in these coordinates is no longer valid, and point Q_i should not be taken into account.

Denoting

$$\mathbf{A}_i = \begin{pmatrix} p_i^2 & 2p_i q_i & q_i^2 \\ p_i & q_i & 0 \\ 0 & p_i & q_i \end{pmatrix}, \qquad \mathbf{b}_i = \begin{pmatrix} 2n_i \\ -\alpha_i \\ -\beta_i \end{pmatrix}, \qquad \mathbf{x} = \begin{pmatrix} e \\ f \\ g \end{pmatrix},$$

the measurement Eqs. (E_1–E_3) at P can be put in matrix form

$$\mathbf{A}_i \mathbf{x} = \mathbf{b}_i.$$

3.2 Non-recursive minimum variance least-squares solution

We wish to weight the measurement equations by the uncertainty of our measured parameters, i.e., the coordinates of points Q_i and attached normals $\mathbf{n}_i$. Once this is done (cf. next sections), we end up with a matrix $\mathbf{W}_i$ which is the covariance of $\mathbf{A}_i\mathbf{x} - \mathbf{b}_i$

$$\mathbf{W}_i = E\left[(\mathbf{A}_i\mathbf{x} - \mathbf{b}_i)(\mathbf{A}_i\mathbf{x} - \mathbf{b}_i)^t\right].$$

Then a weighted least-squares solution $\mathbf{x}$ to our problem at P using all $Q_i, i = 1, \ldots, n$ in some neighbourhood will therefore minimize

$$C = \sum_i (\mathbf{A}_i\mathbf{x} - \mathbf{b}_i)^t \mathbf{W}_i^{-1} (\mathbf{A}_i\mathbf{x} - \mathbf{b}_i),$$

[1] A common enough assumption throughout computer vision.

and is given by

$$\mathbf{x} = \left(\mathbf{A}^t\mathbf{W}^{-1}\mathbf{A}\right)^{-1}\mathbf{A}^t\mathbf{W}^{-1}\mathbf{b},$$

where

$$\mathbf{A} = \begin{pmatrix} \mathbf{A}_1 \\ \vdots \\ \mathbf{A}_n \end{pmatrix}, \qquad \mathbf{b} = \begin{pmatrix} \mathbf{b}_1 \\ \vdots \\ \mathbf{b}_n \end{pmatrix}, \qquad \text{and} \quad \mathbf{W} = \begin{pmatrix} \mathbf{W}_1 & & \\ & \ddots & \\ & & \mathbf{W}_n \end{pmatrix}.$$

3.3 Recursive solution

In fact, we implement a recursive solution to this problem, better known as a *Kalman filter* [Lue69, Aya91]. By this method, each time a new measurement Q_i is given, it is only necessary to compute $\mathbf{A}_i$ and $\mathbf{b}_i$ *for that point* and to update the current solution $(\mathbf{x}_i, \mathbf{S}_i)$ using the recursive equations

$$\begin{cases} \mathbf{x}_i &= \mathbf{x}_{i-1} + \mathbf{K}_i(\mathbf{b}_i - \mathbf{A}_i\mathbf{x}_{i-1}), \\ \mathbf{K}_i &= \mathbf{S}_{i-1}\mathbf{A}_i^t(\mathbf{W}_i + \mathbf{A}_i\mathbf{S}_{i-1}\mathbf{A}_i^t)^{-1}, \\ \mathbf{S}_i &= (\mathbf{I} - \mathbf{K}_i\mathbf{A}_i)\mathbf{S}_{i-1}. \end{cases}$$

$\mathbf{S}_i$ is the *parameter* covariance matrix

$$\mathbf{S}_i = E\left[(\mathbf{x}_i - \mathbf{x})(\mathbf{x}_i - \mathbf{x})^t\right]$$

relating the current estimate $\mathbf{x}_i$ and the ideal value $\mathbf{x}$ of the parameter vector. This is a measure of the quality of our estimate — a small covariance means that the computed estimate $\mathbf{x}_i$ is expected to lie close to the "actual" parameters $\mathbf{x}$. It is necessary to initialize the filter with $(\mathbf{x}_0, \mathbf{S}_0)$, which can be taken as $\mathbf{x}_0 = \mathbf{0}, \mathbf{S}_0 = \infty\,\mathbf{I}$ when *no a priori* information is available about any of the parameters.

3.4 Practical details

For simplicity, the preceding development was presented with all data assumed to be in P's tangent plane coordinate system. We now show how to transform from the actual data points Q_i and normal vectors $\mathbf{n}_i$, each with their respective associated covariance matrices $\mathbf{W}_Q$ and $\mathbf{W}_\mathbf{n}$, measured in a *global* coordinate system, i.e., the coordinate system of the image, to variables $\mathbf{v} = (p_i, q_i, n_i, \alpha_i, \beta_i)^t$ and associated covariance matrix $\mathbf{W}_i$ in P's tangent plane coordinates. Thus we can apply the above theory directly to the image data.

3.4.1 Computing parameters v

We now assume that $Q_i = (x_i, y_i, z_i)^t$ and $\mathbf{n}_i = (n_{x_i}, n_{y_i}, n_{z_i})^t$ are given in a global coordinate system $(\mathbf{X}, \mathbf{Y}, \mathbf{Z})$. To express them in P's tangent plane coordinates $(\mathbf{P}, \mathbf{Q}, \mathbf{N})$ at point $P = (x, y, z)^t$, we compute

$$\begin{pmatrix} p_i \\ q_i \\ n_i \end{pmatrix} = \mathbf{R}\begin{pmatrix} x_i - x \\ y_i - y \\ z_i - z \end{pmatrix}, \qquad \begin{pmatrix} \alpha_i' \\ \beta_i' \\ \gamma_i' \end{pmatrix} = \mathbf{R}\begin{pmatrix} n_{x_i} \\ n_{y_i} \\ n_{z_i} \end{pmatrix},$$

and

$$\alpha_i = \frac{\alpha_i'}{\gamma_i'}, \qquad \beta_i = \frac{\beta_i'}{\gamma_i'},$$

for

$$\mathbf{R} = \begin{pmatrix} P_x & P_y & P_z \\ Q_x & Q_y & Q_z \\ N_x & N_y & N_z \end{pmatrix}.$$

The coordinates of the tangent plane basis vectors at P expressed in the global image coordinates $(\mathbf{X}, \mathbf{Y}, \mathbf{Z})$ are

$$\mathbf{P} = \begin{pmatrix} P_x \\ P_y \\ P_z \end{pmatrix}, \qquad \mathbf{Q} = \begin{pmatrix} Q_x \\ Q_y \\ Q_z \end{pmatrix}, \qquad \mathbf{N} = \begin{pmatrix} N_x \\ N_y \\ N_z \end{pmatrix}.$$

3.4.2 Computing covariances $\mathbf{W}_i$

We assume that the covariance of point Q_i and its normal $\mathbf{n}_i$ are given in the *global coordinate system* $(\mathbf{X}, \mathbf{Y}, \mathbf{Z})$ by $\mathbf{W}'_{Q_i}$ and $\mathbf{W}'_{\mathbf{n}_i}$ respectively. Since, for any affine transformation of a random variable $\mathbf{v}_i \rightarrow \mathbf{w}_i = \mathbf{M}(\mathbf{v}_i - \mathbf{v})$ we have

$$E\left[(\mathbf{w}_i - \mathbf{w})(\mathbf{w}_i - \mathbf{w})^t\right] = \mathbf{M}\, E\left[(\mathbf{v}_i - \mathbf{v})(\mathbf{v}_i - \mathbf{v})^t\right] \mathbf{M}^t,$$

the corresponding covariance matrices expressed in P's tangent plane coordinate system $(\mathbf{P}, \mathbf{Q}, \mathbf{N})$ are

$$\mathbf{W}_{Q_i} = \mathbf{R}\mathbf{W}'_{Q_i}\mathbf{R}^t, \qquad \mathbf{W}_{\mathbf{n}_i} = \mathbf{R}\mathbf{W}'_{\mathbf{n}_i}\mathbf{R}^t,$$

which are 3×3 matrices.

In fact, if we express $\mathbf{n}_i = (\alpha'_i, \beta'_i, \gamma'_i)^t$ in the tangent plane coordinates, we must compute the covariance of $\alpha_i = \alpha'_i/\gamma'_i$ and $\beta_i = \beta'_i/\gamma'_i$. As a first order approximation, we compute the 2×2 matrix $\widetilde{\mathbf{W}}_{\mathbf{n}_i}$

$$\widetilde{\mathbf{W}}_{\mathbf{n}_i} = \mathbf{J}_1 \mathbf{W}_{\mathbf{n}_i} \mathbf{J}_1^t$$

where $\mathbf{J}_1$ is the Jacobian matrix

$$\mathbf{J}_1 = \begin{pmatrix} \frac{1}{\gamma'_i} & 0 & \frac{-\alpha'_i}{\gamma'^2_i} \\ 0 & \frac{1}{\gamma'_i} & \frac{-\beta'_i}{\gamma'^2_i} \end{pmatrix}$$

of the change of variables. Therefore the 5×5 matrix

$$\mathbf{W}_{Q,\mathbf{n}} = \begin{pmatrix} \mathbf{W}_Q & \mathbf{0}_{3\times 2} \\ \mathbf{0}_{2\times 3} & \widetilde{\mathbf{W}}_{\mathbf{n}_i} \end{pmatrix}$$

is the covariance of our measurement vector $(p_i, q_i, n_i, \alpha_i, \beta_i)$.

The 3×3 covariance matrix $\mathbf{W}_i$ is computed as a first order approximation by

$$\mathbf{W}_i = \mathbf{J}_2 \mathbf{W}_{Q,\mathbf{n}_i} \mathbf{J}_2^t,$$

where $\mathbf{J}_2$ is the Jacobian matrix

$$\mathbf{J}_2 = \begin{pmatrix} 2p_i e + 2q_i f & 2p_i f + 2q_i g & -2 & 0 & 0 \\ e & f & 0 & 1 & 0 \\ 0 & f & g & 0 & 1 \end{pmatrix}.$$

The 2×2 covariance matrix of curvatures is determined similarly,

$$\mathbf{W}_c = \mathbf{J}_3 \mathbf{W}_{Q_i} \mathbf{J}_3^t,$$

with the Jacobian

$$\mathbf{J}_3 = \begin{pmatrix} c & -2b & a \\ \frac{1}{2} & 0 & \frac{1}{2} \end{pmatrix}.$$

4 Estimating error in edge detection

In the reference [MDMC, MAS91], we determine the uncertainty inherent in edge detection in digital images by considering the 3-D (modified Canny) edge detector of Monga and Deriche [MD89, MDR91]. We first deal with uncertainty in edge position, and then with the error in edge direction and magnitude. We determine precisely the covariance matrices needed for the local quadric surface fitting described above, and derive the very interesting result that the uncertainty in edge position and magnitude is highly dependent on the orientation of the edge with respect to the image coordinate axes.

5 From curvatures to typical features

5.1 Introduction

For each edge point, the previous section determines the Gaussian and mean curvatures, principal curvature directions, and the corresponding covariance matrices. Note that the scale is defined by the size of the neighbourhood used to fit the local geometric model. In this section we deal with the extraction of more global curvature features from the local curvature information.

5.2 Local curvature maps

A practical way of characterizing the behaviour of the curvature in the neighbourhood of a point is to define local curvature maps (technically the pullback of the field onto the tangent plane as used in [SZ] for the computation of the direction field index). Given a point P and its tangent plane defined by $(\mathbf{P}, \mathbf{Q}, \mathbf{N})$. Let V be the intersection of a sphere whose center is P and radius r with the set of the edge points (this defines a neighbourhood of P), and let W be the orthogonal projection of the points of V onto the tangent plane. At each point of W we attach the curvatures of its corresponding points in V. The size of V could be determined using the distance of the points to the tangent plane and the angle between the gradient at a point and the gradient at point P. We thus define a map characterizing the behaviour of the curvatures around P.

5.3 Extracting lines of curvature extrema

From the local curvature images we can extract, for instance, the maxima of the maximum curvature in the maximum curvature direction . This may be done similarly to the classical extraction of the extrema of the gradient magnitude in the gradient direction in 2D edge detection methods [Der87, Can86].

Let $C(P)$ be the local maximum curvature map attached to point P, and let $G(P)$ be the maximum curvature direction. We compare the value of the maximum curvature along the straight line defined by P and $G(P)$ and retain P if its maximum curvature is a local extrenum along this direction. Thus we obtain local curvature extrema candidates. To remove false extrema, we perform a 3D hysteresis thresholding using the mean curvature already determined. This is done analogously to the thresholding of the local gradient extrema in the edge detection scheme described in [MDR91].

6 Results

6.1 Curvatures for synthetic data

We built a synthetic volume whose implicit equation is given by

$$z \leq ax^2 + by^2 + cx + dy + e$$

with $a = 1/20$, $b = 0.25$, $c = -4$, $d = -12$, $e = 224$. This was done by creating a 3-D digital image with points of maximum (resp. minimum) intensity within (resp. outside of) the volume. We extracted 3-D edges with the algorithm described in [MDR91]. These edge points correspond to the surface of an ideal elliptic paraboloid.

First, note that there exists a single surface point T such that the equation of the *entire* surface takes the reduced form

$$z' = \frac{1}{2}ex'^2 + fx'y' + \frac{1}{2}gy'^2$$

when (x',y',z') are expressed in the local tangent plane coordinate system attached to point T. This point is the vertex of the paraboloid and its coordinates are given by

$$T = (\frac{-c}{2a}, \frac{-d}{2b}, \frac{-c^2}{4a} - \frac{d^2}{4b} + e).$$

Point coordinates	Ideal	Positions	+ Normals	+ Uncertainty	Predicted σ
	$e = 0.1$	− 0.0037	0.0172	0.102	0.011
(40,24,1)	$f = 0$	0.0000	0.000	− 0.003	0.008
86 Neighbors	$g = 0.5$	0.324	0.360	0.494	0.02

Table 1: Estimation of the parameters (e, f, g) of the local quadrics

Point coordinates	Ideal	Positions	+ Normals	+ Uncertainty	Predicted σ
(40,24,1)	$C_g = 0.05$	− 0.0012	0.0062	0.0505	0.014
86 Neighbors	$C_m = 0.3$	0.16	0.16	0.298	0.023
(47,24,2)	$C_g = 0.022$	0.089	0.063	0.0157	0.008
46 Neighbors	$C_m = 0.23$	0.333	0.297	0.2024	0.030
(45,26,3)	$C_g = 0.010$	− 0.001	− 0.0003	0.018	0.009
54 Neighbors	$C_m = 0.12$	0.053	0.107	0.143	0.018
(36,22,2)	$C_g = 0.010$	0.013	0.018	0.012	0.006
50 Neighbors	$C_m = 0.122$	0.133	0.172	0.127	0.015
(39,23,1)	$C_g = 0.031$	0.011	0.023	0.017	0.023
28 Neighbors	$C_m = 0.22$	0.10	0.25	0.21	0.062
(38,28,5)	$C_g = 0.004$	0.009	0.010	0.006	0.003
50 Neighbors	$C_m = 0.07$	0.105	0.11	0.09	0.01

Table 2: Estimation of gaussian and mean curvatures C_g and C_m

For this particular point, the local quadric approximation is a *global* one, and the ideal parameters are $e = 2a$, $f = 0, g = 2b$. It is therefore possible to estimate these parameters with all the detected surface points (about 350 points). In this case the convergence is excellent towards the exact values. We show in table 1 the results obtained with a smaller but still rather large number of edge points (86). We show successively the results obtained for a least squares estimation with points only (measurement equation E1), then adding normals (measurement equations E2–E3). Finally, we show the results obtained when uncertainty on positions and normals is taken into account, following the computations of the previous sections. It is easy to check that not only is the estimate obtained much more accurate, but also that the computed standard deviation σ on the error estimation is perfectly coherent with the observed error.

At other points P on the surface, we applied our local quadric approximation with smaller neighborhoods (containing about 50 points). The size of the neighborhood is both controlled by limiting the angle between the neighbors' normal and P's normal, and also the distance between neighbors and P. We used the local approximation to compute locally the Gaussian and mean curvatures (C_g and C_m). In table 2, we show the results obtained for this computation, with the previous three methods. Here again, the results are much more accurate with the last approach, and the output covariance agrees almost perfectly well with the observed errors.

6.2 Typical curvature features for synthetic and real data

Figures 1 to 5 present some results for the determination of the extrema of the maximum curvature in the maximum curvature direction for a 3D MRI image of the face. We notice that our local approximation scheme provides a continuous maximum curvature field, allowing to detect reliably and accurately the curvature extrema. Regarding our experiences, this continuity is mainly due to the smoothness of the orientation of the gradient used for the local approximation.

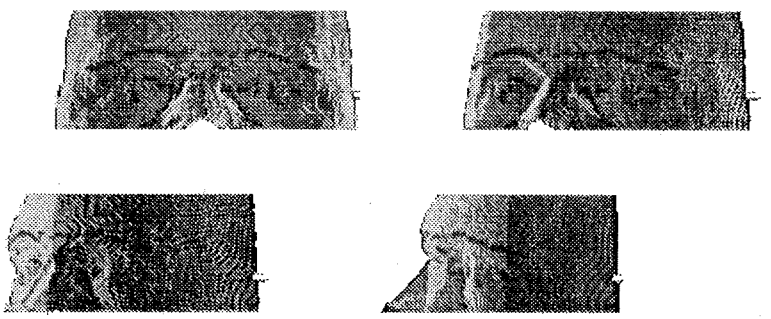

Figure 1: Perspective views of the 3D edges matched with the extrema of the maximum curvature in the maximum curvature direction colored in dark (the ratio defining the weighting point/normal in the least mean squares is about 1/40)

Using covariance matrices in our least mean square criterion introduces a ponderation between the equations taking into account the position of the points and the normal orientations. For the original data corresponding to figures 1 to 5 the step edges have a very strong amplitude. This implies that the localization criterion is over-estimated due to the first order approximation (the localization is inversely proportional to the step amplitude), and therefore the weight put on the position equations is too high. We also remark that the gradient coordinates are real values but that the point coordinates are integer values which could induce false discontinuity. Given that each point produces one measurement equation using its position and two measurement equations using the orientation of its gradient, we can evaluate the ratio between point information and normal information. If we apply exactly the theoretical calculus presented before for these data, we obtain a ratio of 1/12 (1 for point and 12 for normal). This allows to obtain rather good results but where some false discontinuities still remain. Experimentally a ratio of 1/40 yields a good trade-off between the smoothness and the preservation of the singularities. The distorsion of the theoretical optimum and the experimental one is due to the reasons we reported here. We also perform some experiences with a ratio of 1/4 and we obtain a bad continuity for the maximum curvature field.

The main practical conclusion of our experiences is that the gradient orientation (approximating the orientation of the normal to the surface) is a strong regularization criteria for the local approximation. This illustrate the applicability of our theoretical developments although its direct applicability are spoiled by first order approximations and by discretization.

7 Conclusion

Our main objective was to develop robust and reliable tools useful for modeling and analyzing surfaces of 3-D objects. In this paper we showed the importance of a careful quantitative analysis of the various sources of uncertainty for computing second order derivative features (mean and Gaussian curvatures) on a discrete surface.

We use a quantitative estimation of the uncertainty in edge position, orientation and magnitude produced by the multidimensional (2-D and 3-D) versions of the Monga-Deriche-Canny recursive separable edge-detector.

Figure 2: Projection of the extrema of the maximum curvature in the maximum curvature direction corresponding to the previous figure (the ratio defining the weighting point/normal in the least mean squares is about 1/40)

Figure 3: Projection of the extrema of the maximum curvature in the maximum curvature direction (the ratio defining the weighting point/normal in the least mean squares is about 1/40) ; the algorithm providing the extrema is slightly different.

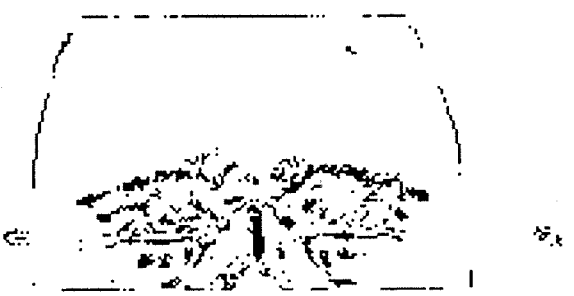

Figure 4: Projection of the extrema of the maximum curvature in the maximum curvature direction (the ratio defining the weighting point/normal in the least mean squares is about 1/320)

Figure 5: Projection of the extrema of the maximum curvature in the maximum curvature direction (the ratio defining the weighting point/normal in the least mean squares is about 1/5)

Then, we revisited the algorithm initially proposed by Sander and Zucker for locally estimating the curvature of a discrete 3-D surface, and we modified the original measurement equations and proposed an optimal estimation scheme to account for the previously computed uncertainties and corrections.

We tested the corrected edge detector on 2-D and 3-D medical images and showed the importance of the corrected edge magnitude for edge detection. We also tested the surface modeling algorithm on discrete 3-D objects — not only are the results obtained more accurate, but the computed measure of uncertainty attached to the results agrees extremely well with the true one.

We also show how to use these curvatures to determine typical curvature features on which registration and/or tracking procedures can robustly rely.

Acknowledgements

We thank Serge Benayoun for the implementation of the extraction of the local curvature extrema. Nathalie Gaudechoux provided a substantial help in the preparation of this manuscript.

We thank Pr. Bittoun of the Kremlin Bicetre Hospital in Paris and Pr. J.L. Coatrieux in Rennes which provided the medical images.

This work has been partially supported by Ge-Cgr and some of the presented images were acquired in collaboration with the Advanced Image Processing Group of GE-CGR in Buc, France. We shall give the details of this acquisition process, and a thorough description of the results very soon in a forthcoming joint paper Inria-Ge-Cgr. This work was also partially supported by Digital Equipment Corporation and European AIM (Advanced Informatics in Medicine) Project Murim.

References

[AB+90] N. Ayache, J.D. Boissonnat, , L. Cohen, , B. Geiger, J. Levy-Vehel, O. Monga, and P. Sander. Steps toward the automatic interpretation of 3d images. In *Proceedings of the NATO Advanced Research Workshop on 3D Imaging in Medicine*, Travemünde, June 1990. NATO ASI Series, Springer-Verlag.

[Aya91] N. Ayache. *Artificial Vision for Mobile Robots – Stereo-Vision and Multisensory Perception.* MIT Press, Boston, 1991.

[BJ88] Paul J. Besl and Ramesh C. Jain. Segmentation through Variable-Order surface fitting. *IEEE Transactions on Pattern Analysis and Machine Intelligence*, PAMI-10(2):167–192, March 1988.

[Can86] John Canny. A computational approach to edge detection. *IEEE Transactions on Pattern Analysis and Machine Intelligence*, PAMI-8(6):679–698, November 1986.

[dC76] Manfredo P. do Carmo. *Differential Geometry of Curves and Surfaces.* Prentice-Hall, Englewood Cliffs, 1976.

[Der87] Rachid Deriche. Using Canny's criteria to derive a recursively implemented optimal edge detector. *International Journal of Computer Vision*, pages 167–187, 1987.

[Koe90] Jan J. Koenderink. *Solid Shape.* MIT Press, Boston, 1990.

[Lue69] David G. Luenberger. *Optimization by Vector Space Methods.* Wiley, New York, 1969.

[MAS91] Olivier Monga, Nicholas Ayache, and Peter Sander. From voxel to curvature. Technical report, INRIA, 1991. No 1356.

[MD89] Olivier Monga and Rachid Deriche. 3d edge detection using recursive filtering. In *Conference on Vision and Patern Recognition*, San Diego, June 1989. IEEE.

[MDMC] Olivier Monga, Rachid Deriche, Gregoire Malandain, and Jean-Pierre Cocquerez. Recursive filtering and edge closing: two primary tools for 3d edge detection.

[MDR91] Olivier Monga, Rachid Deriche, and Jean-Marie Rocchisani. 3d edge detection using recursive filtering: Application to scanner images. *Computer Vision Graphic and Image Processing, Vol. 53, No 1, pp. 76-87*, January 1991.

[SZ] Peter T. Sander and Steven W. Zucker. Singularities of principal direction fields from 3-D images. *IEEE Transactions on Pattern Analysis and Machine Intelligence.* To appear. Available as Technical Report CIM-88-7, McGill Research Center for Intelligent Machines, McGill University, Montréal.

[SZ87] Peter T. Sander and Steven W. Zucker. Tracing surfaces for surfacing traces. In *Proceedings of the First International Conference on Computer Vision*, pages 241–249, London, June 1987.

[SZ90] Peter T. Sander and Steven W. Zucker. Inferring surface trace and differential structure from 3-D images. *IEEE Transactions on Pattern Analysis and Machine Intelligence*, 12(9), September 1990.

[ZH81] S.W. Zucker and R.M. Hummel. A three-dimensional edge operator. *IEEE Transactions on Pattern Analysis and Machine Intelligence*, PAMI-3(3):324–331, May 1981.